Proceedings of the XVIII ECSMGE 2024
GEOTECHNICAL ENGINEERING CHALLENGES
TO MEET CURRENT AND EMERGING NEEDS OF SOCIETY

ISBN 978-1-032-54816-6
DOI 10.1201/9781003431749-526

ECSMGE 24
XVIII EUROPEAN CONFERENCE ON SOIL MECHANICS AND GEOTECHNICAL ENGINEERING

3D small-scale tests on steel-reinforced piled embankments

Essais sur modèles réduits en 3D de remblais sur pieux renforcés par une nappe de treillis soudés

S.J.M. van Eekelen*
Deltares, Netherlands

M. Schneider
Technical University of Darmstadt, Institute of Geotechnics, Germany

B. Wittekoek
Deltares, Netherlands

M. Hell, P. Pandrea
Keller, Germany

P. Schauber
Keller, France

M. Topolnicki
Keller, Poland

K. Makowska
SHM System, Poland

K. Zdanowicz
SHM System, Poland / FOLAB GmbH, Germany

R. Sieńko
SHM System, Poland

H. Zachert
Technical University of Darmstadt, Institute of Geotechnics, Germany

suzanne.vaneekelen@deltares.nl

ABSTRACT: This paper looks at the behaviour of welded steel mesh-reinforced piled embankments through a series of small-scale tests. Findings reveal that reinforcement axial and bending stiffnesses have minimal influence on soil arching. In contrast, the friction angle of the embankment fill plays a more significant role in shaping soil arching. The Concentric Arches (CA) model, adopted in CUR226 (2016), tailored for geosynthetics, matches the measured soil arching well. The study introduces the use of Distributed Fibre Optic Sensing (DFOS) technology, providing a 3D view of reinforcement and fill deformations.

RÉSUMÉ: Cet article examine le comportement de remblais en pieux renforcés par treillis soudés à travers une série de tests à petite échelle. Les résultats révèlent que la rigidité du renforcement a une influence minimale sur les transferts de charges. En revanche, l'angle de frottement du matériau de remblai joue un rôle plus significatif dans les mécanismes de transferts de charges. L'effet d'arche du modèle 'Concentric Arches' (CA), utilisé dans CUR226 (2016), dédiée aux géosynthétiques correspond bien aux mesures obtenues. L'étude introduit également l'utilisation de la technologie de détection par fibre optique répartie (DFOS), offrant une vision tridimensionnelle des déformations du renforcement et du remblai.

Keywords: Piled embankments; steel basal reinforcement; model scale tests; soil arching.

1 STEEL MESH BASAL REINFORCEMENT IN PILED EMBANKMENTS

Pile-supported (PS) embankments with basal geosynthetic reinforcement (GR) are commonly built in soft soil areas (van Eekelen and Han, 2020). Steel mesh reinforcement (SR) is particularly appealing for high embankments (Topolnicki et al., 2019). Its high axial stiffness, in comparison to geosynthetic, reduces horizontal deformation at the embankment base, minimizes bending moments in the piles, ultimately enhancing the embankment stability.

This paper presents a small-scale test series on steel-reinforced piled embankments, conducted in the Deltares laboratory. The tests are part of a broader research initiative called Piled Embankments with Basal Steel Reinforcement (PEBSTER), which also includes a large-scale test (Schneider et al., 2024).

The research aims to address the following questions:

1. Does the soil arching in a piled embankment differ if SR is used instead of GR?
2. Are deformations different with SR instead of GR?
3. What is the influence of flexible vs. rigid piles?
4. Can the current design methods for piled embankments using GR be applied for SR or do they require a modification?
5. Do the answers on these questions depend on the scale of model tests?

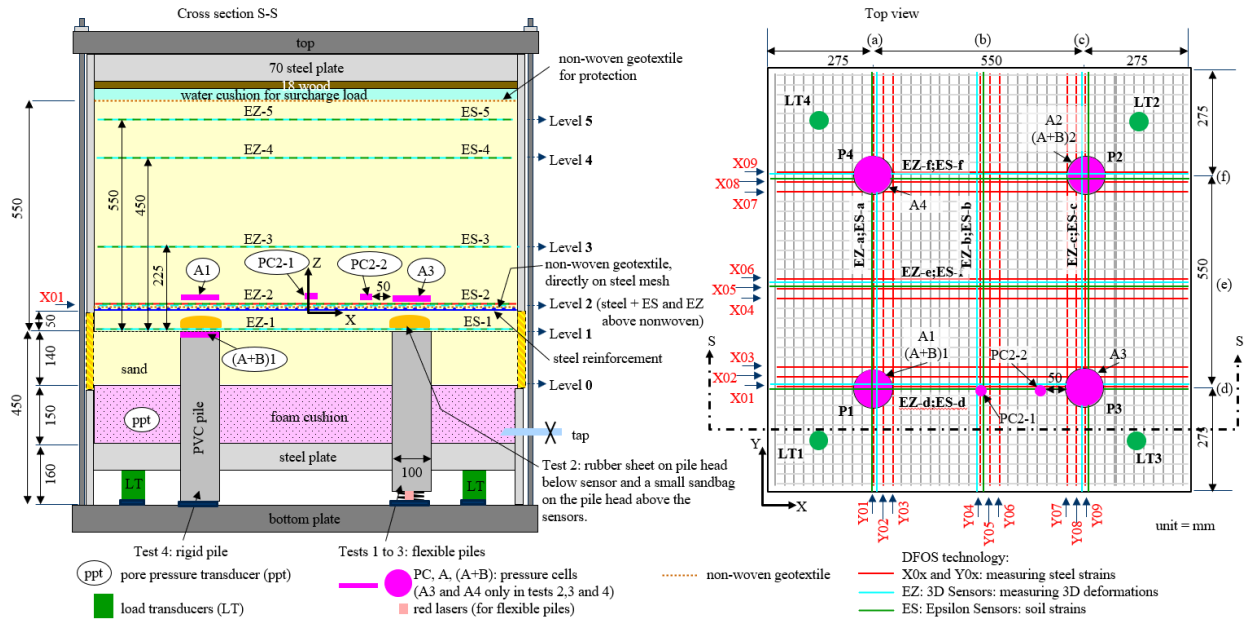

Figure 1. Test set-up small scale test steel-reinforced pile-supported embankments.

2 SET-UP SMALL SCALED TESTS

Figure 1 shows the test set-up, which is an extended version of the test set-up described by Van Eekelen et al. (2012a, 2024a). A steel plate supports a foam cushion, that is sealed and soaked. A tap allows for drainage of the foam cushion, simulating the consolidation of the subsoil between the piles. Four piles with a 0.1 m diameter pass through the steel plate.

The welded steel mesh-reinforcement was placed 50 mm above the pile heads. It consists of 43 bars in each direction. These bars have a 5 mm diameter and a centre-to-centre spacing of 25 mm, resulting in the axial stiffness EA = 164934 kN/m and bending stiffness EI = 0.2577 kN·m^2.

The fill material used is 'Darmstadt sand', sediments from the river Main, characterized as medium coarse sand. Table 1 lists test details, where the values of φ'_{cv} were derived from the relative density (RD) of the fill, using an empirical correlation obtained from 15 triaxial tests.

Table 1. Test details of the four small-scale tests.

Test no.	**1**	**2**	**3**	**4**
Fill height above steel (m)	0.55	0.55	0.55	0.56
Unit weight γ (kN/m^3)	16.7	16.9	17.0	16.6
Relative density RD (%)	68	72	75	64
Friction angle φ'_{cv} (°)	33.8	34.0	34.1	33.7

An equally distributed surcharge load is applied using a water cushion. A rubber sheet greased with Vaseline minimises the friction between fill, box walls, foam cushion and piles. The load distribution is measured by pressure cells and load transducers.

Soil strains and displacements were monitored at five elevations within the fill (Figure 1), utilizing distributed fibre optic sensing (DFOS) technology from the Nerve-Sensors family, as depicted in Figure 2. Additionally, the steel mesh reinforcement was extensively instrumented with optic fibres. In the x-direction, X01 to X09 were glued to the top of the top steel bars, while in the y-direction, Y01 to Y09 were attached to the bottom of the bottom steel bars.

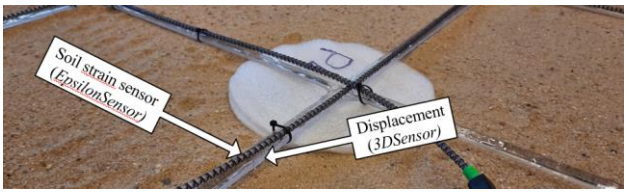

Figure 2. DFOS sensors (connected to a LUNA OBR 4600 reflectometer with 15-channel optical switch).

The series of four tests included:

Test 1: With SR, flexible piles (utilizing springs with a stiffness of 4605 kN/m below the piles) and stepwise consolidation;

Test 2: As Test 1, but continuous consolidation (the tap of the foam cushion was kept open permanently). This test closely aligns with the large-scale test described by Schneider et al., 2024.;

Test 3: As Test 1, but without SR;

Test 4: As Test 1, but with rigid piles (no springs).

3 MEASURED LOAD DISTRIBUTION

When the area between the piles deforms more than the piles, soil arching develops. In a piled embankment

with basal reinforcement, this results in a non-uniform distribution of the vertical load on the reinforcement. A significant portion of the vertical load (labelled as 'A' in Figure 3) is directly transferred to the piles since they deform less than the reinforcement. The residual load, 'B+C' in Figure 3, is supported by the subsurface between the piles.

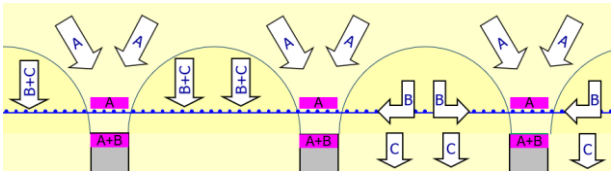

Figure 3. Load distribution in a PS embankment.

Several design guidelines and standards, such as BS8006 (2010), EBGEO (2011), ASIRI (2012), CUR226 (2016), and Topolnicki and Kłosiński et al. (2022), provide equations to divide the total vertical load into A and B+C. These guidelines then offer methods for calculating the strain in the reinforcement from B+C, considering the load-deflection behaviour of the reinforcement.

Many researchers have analysed how the geometry and material properties affect soil arching. Van Eekelen et al. (2012b) showed that the soil arching quickly develops, even when the deflection of the GR is minimal. In line with this finding, they showed that the GR tensile stiffness has a limited impact on soil arching, while the shear properties of the fill (internal friction angle) play a significant role.

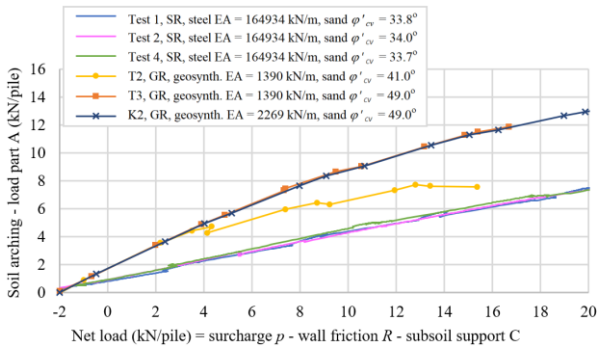

Figure 4. Measured soil arching A in the current tests with SR, compared to previous tests with GR in the same test box (van Eekelen et al., 2012).

These conclusions were valid for GR. An important question is whether the high axial and bending stiffnesses of the SR affect the soil arching.

Figure 4 compares Tests 1, 2 and 4 with SR with three previous tests with GR, conducted in the same test box. The data show much less soil arching in the SR tests than in the GR tests. The fill friction angle, however, seems to have a major impact on the soil arching, where the reinforcement stiffness does not show the same level of influence.

Since only one combination of SR stiffness and fill friction angle was tested, the pure test results cannot confirm this conclusion. However, it is possible to validate the impact of the fill and SR stiffness by comparing the measured and calculated soil arching, using three analytical methods, as shown in Figure 5 for four conducted tests.

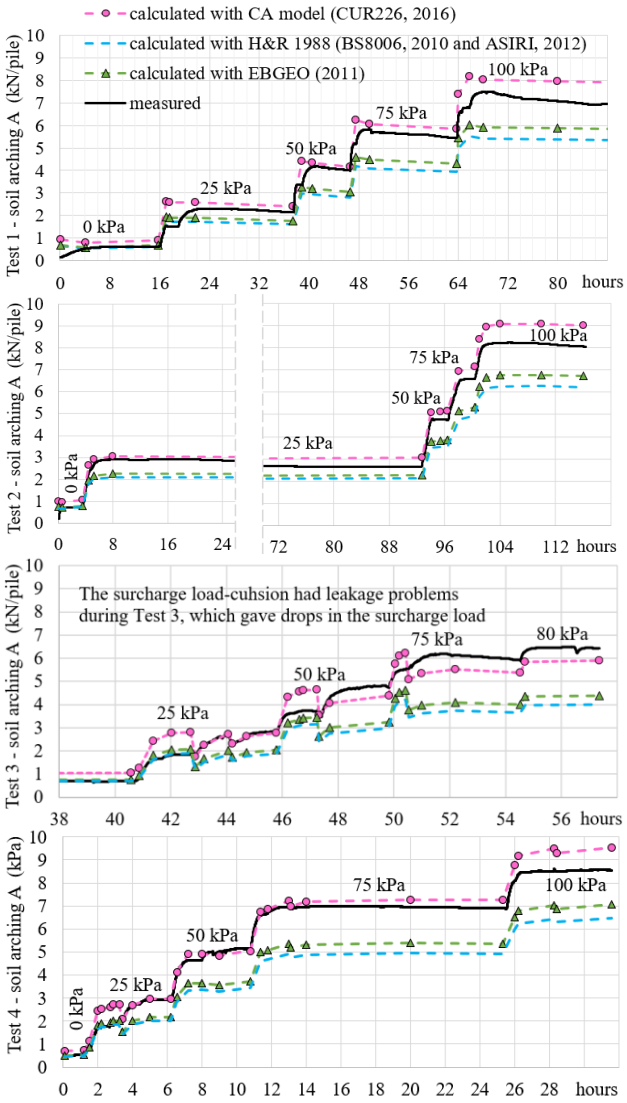

Figure 5. Measured and calculated soil arching A, using three European models. H&R refers to the model of Hewlett & Randolph 1988. Surcharge loads are indicated (0 to 100 kPa). Input parameters from Table 1.

The CA model (CUR226, 2016) consistently matches the measurements well, specifically for $p \leq 75$ kPa. It can therefore be concluded that the axial and bending stiffnesses of the reinforcement do not play a significant role because they are not considered in the soil arching part of the CA model.

4 MEASURED FILL DEFORMATIONS

For each test, the model was rebuilt. Some DFOS ruptured during testing (due to high local strains above 4%), and not all of them could be replaced in the next test. For this reason, this section focuses on Test 1, although Tests 1, 2 and 4 exhibit similar trends. This becomes evident when comparing Figure 6 and Figure 7, for example.

Figure 6 and Figure 7 show the settlements measured at different levels in the fill. The most significant differential settlements occur in the steel bars that bridge adjacent piles, denoted by lines (a), (c), (d) and (f).

The bars running through the centre of the test setup, represented by lines (b) and (e), show slightly more settlement, but notably less differential settlement. After the consolidation phase under a surcharge load of 25 kPa, the maximum settlement of the steel mesh (level 2), in the centre between four piles, is on average 8.6% greater than the settlement in the middle between adjacent piles. This finding is in line with the 3D FEM analysis of Zhang et al. (2019), who reported 6 to 8% difference. In contrast, the field measurements of Van Eekelen et al. (2020) showed a difference of approximately 25%.

The differential deflection of the steel mesh (level 2) between the piles causes soil arching. At level 3, located 225 mm above the pile heads, the differential settlement is noticeably less. At levels 4 and 5, it was only possible to reliably assess the deformations along lines (b) and (e). The settlements at these lines (b) and (e) at levels 4 and 5 are uniform. This does not prove that the 'plane of equal settlement' has been found, as there is no information about lines (a), (c), (d) and (f) at these high elevations, and these are the lines where most differential settlement occur.

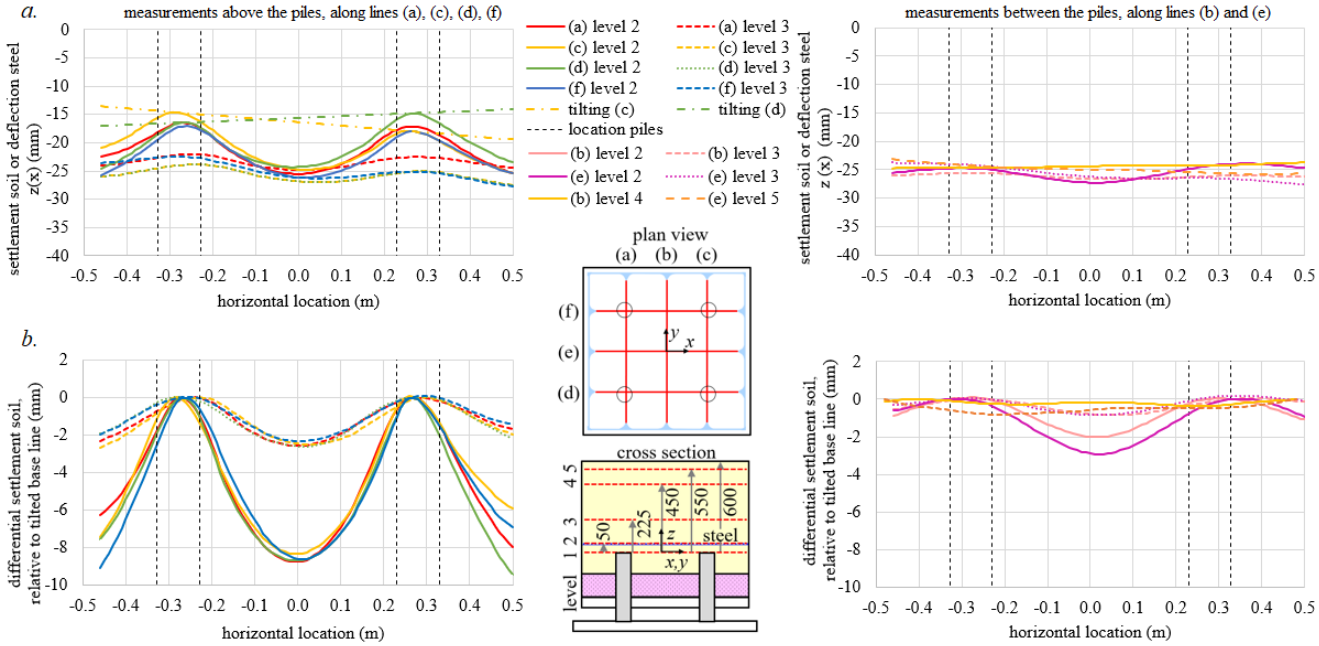

Figure 6. Test 1. Measured settlement in the fill at various levels under a 25 kPa surcharge load, after a consolidation phase. a. Measured settlements b. Settlement relative to the tilting baselines of each grid, as illustrated in top-left graph.

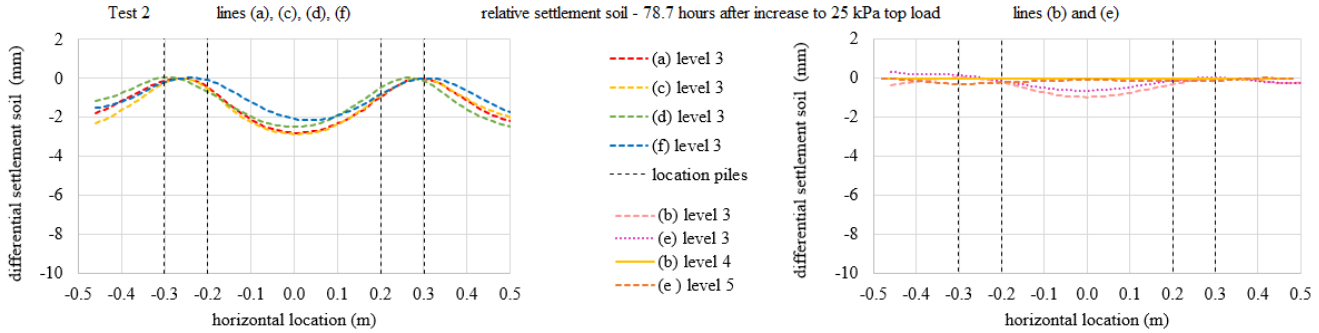

Figure 7. Test 2. Measured settlement in the fill at different levels at 25 kPa surcharge load after a consolidation phase. No data available for Test 2 – level 2.

5 MEASURED STEEL STRAINS

Figure 8 shows the strain at the top of the upper bars, all in x-direction. The left-side graphs show significantly higher strains in the steel bars above the piles, compared to those located between the piles, as shown in the right-side graphs. Bar X03 lies just next to a pile, resulting in 17 – 35% less tensile strain than the average strain in X01, X02 and X07 to X09 for the phases depicted in Figure 8.

Above the piles, we observe tensile strain in the top of the upper bars, indicated by positive values. These strains result from the bending of the steel bars above the piles. In Figure 8*b*, the maximum tensile strain reaches around 0.2%, while the maximum compression strain is around 0.06%. The presence of a 5 cm layer of sand between the steel mesh and pile heads facilitates a 'smooth' bending of the steel bars, contrasting a scenario where the SR has been installed directly on the pile heads.

In the area between the piles, we observe compression strain, represented by negative values in the top of the top bars. This is also caused by the bending of the steel (visible in Figure 7). This behaviour differs from GR, which experiences only tensile strain. Towards the edges of the piles, the steel bars exhibit an increasing tensile strain.

The alternation of compression and tensile strain underscores the importance of considering axial and bending stiffness of the steel mesh when performing calculations to simulate this situation.

The local spikes in Figure 8 are strain reading anomalies (SRAs), which are disturbances in the DFOS fibres. The higher the local bending, the more SRAs were found in the DFOS measurements. Van Eekelen et al. (2024b) further analysed these SRAs in the DFOS measurements.

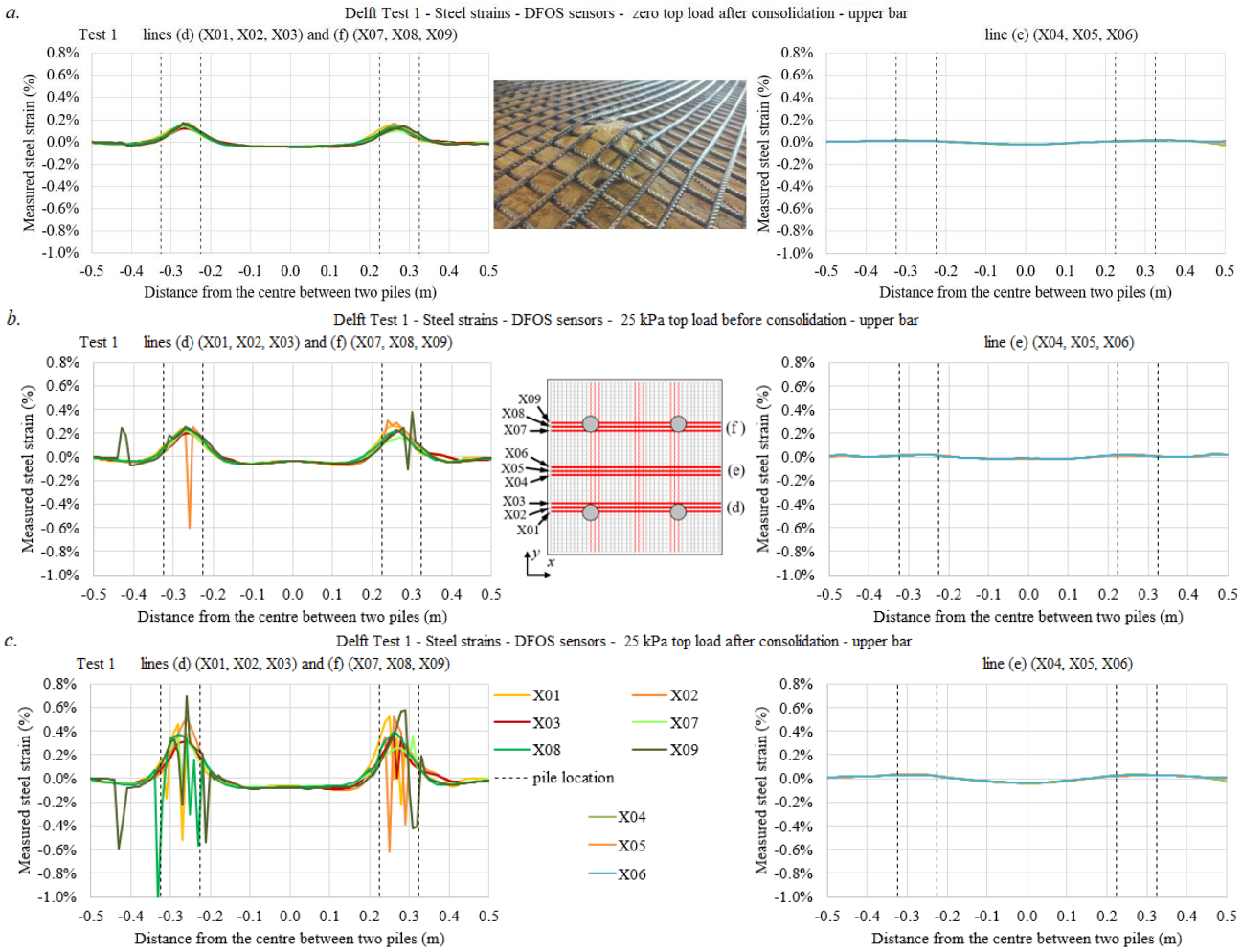

Figure 8. Test 1. Steel strains, measured on top of the top steel bar in x-direction. a. after consolidation without surcharge load, b. after increasing the surcharge load to 25 kPa, and c. after consolidation with surcharge load at 25 kPa.

6 CONCLUSIONS

This paper presents four small-scale tests on steel-reinforced (SR) piled embankments. This is part of a larger research, that also includes a large-scale test and numerical analyses. Based on the test results presented in this paper, we draw the following preliminary conclusions.

- The axial and bending stiffnesses of the SR do not significantly affect the soil arching in the fill above the piles. Consequently, the load part that is transferred to the piles directly (load part A) is similar for both types of basal reinforcement: geosynthetic and welded steel mesh reinforcement.
- The friction angle of the embankment fill has much more influence than the reinforcement type.
- Three main European design methods for GRPS embankments closely align with the measured soil arching, with the CA model exhibiting the best match.
- The DFOS sensors provide continuous and a unique 3D picture of the deformations of the reinforcement and the fill.
- The steel mesh reinforcement shows significant differential deflection and strain in the bars that bridge adjacent piles. The bars running through the centre of the square between the four piles, show slightly more settlement, but much less differential settlement and steel strain. This is in line with the deformation pattern observed in geosynthetic-reinforced piled embankments.
- Tensile strains due to bending are observed above the piles in the top bars of the reinforcement. Compression strains due to bending occur in the area between adjacent piles. This indicates that load-deflection design models for steel mesh and geosynthetic reinforcements should be different.

ACKNOWLEDGEMENTS

The authors are grateful for the funding received from the European Union's Horizon 2020 research and innovation program under Grant Agreement No. 101006512 for the transnational GEOLAB project PEBSTER, the TKI-PPS funding of the Dutch Ministry of Economic Affairs and the financial and practical support of Keller.

REFERENCES

ASIRI (2013). *Recommendations for the design, construction and control of rigid inclusions ground improvements* (French version is of 2012).

BS8006-1 (2010). *Code of practice for strengthened/reinforced soils and other fills*. British Standards Institution, UK.

CUR226 (2016). See van Eekelen and Brugman (2016).

EBGEO (2011). *Recommendations for Design and Analysis for Earth Structures using Geosynthetic Reinforcements* (German version is of 2010).

Hewlett, W.J. and Randolph, M.F. (1988). Analysis of piled embankments. *Ground Eng.,* 21(3): 12-18.

Schneider, M., Hell, M., Wittekoek, B., Pandrea, P., van Eekelen, S.J.M., Topolnicki, M., Makowska, K., Sieńko, R. and Zachert, H. (2024). Large-scale test on the load bearing and deformation behaviour of basal steel-reinforced piled embankments. In: *Proc. ECSMGE 24*, Lisbon, Portugal.

Topolnicki, M., Sołtys, G. and Brzozowski, T. (2019). Performance and modelling of road embankment supported on rigid inclusions and a transfer platform with steel geogrid, *Proc. ECSMGE 2019*, Iceland.

Topolnicki, M., Kłosiński, B. et al. (eds.) (2022). *Recommendations for Ground Improvement with Rigid Inclusions - Design, Execution and Control* (in Polish). PWN SA. ISBN 978-83-01-22578-0.

van Eekelen, S.J.M., Bezuijen, A., Lodder, H.J. and van Tol, A.F. (2012a). Model experiments on piled embankments Part I. *Geotextiles and Geomembranes*, 32: 69-81. DOI: 10.1016/j.geotexmem.2011.11.002.

van Eekelen, S.J.M., Nancey, A. and Bezuijen, A. (2012b). Influence of fill material and type of geosynthetic reinforcement in a piled embankment, model experiments. In: *Proc. Eur. Geosynthetic Congress.,* Valencia, Spain, Vol 5, 167-171.l.

van Eekelen, S.J.M. and Brugman, M.H.A., Eds. (2016). *Design Guideline Basal Reinforced Piled Embankments* (CUR226). CRC press, Delft, Netherlands.

van Eekelen, S.J.M. and Han, J. (2020). Geosynthetic-reinforced pile-supported embankments: state of the art. *Geosynthetics International* 27 (2) 112-141. DOI: 10.1680/jgein.20.00005.

van Eekelen, S.J.M., Venmans, A.A.M., Bezuijen, A. and van Tol, A.F. (2020). Long term measurements in the Woerden geosynthetic-reinforced pile-supported embankment. *Geosynthetics International,* 27 (2) 142-156. DOI: 10.1680/jgein.17.00022.

van Eekelen, S.J.M., Wittekoek, B., Zwaan, R., Bezuijen, A. and Nancey, A. (2024a). Groundwater in geosynthetics-reinforced pile-supported embankments. *Proc. ECSMGE24*, Lisbon, Portugal.

van Eekelen, S.J.M, Schneider, M., Hell, M., Wittekoek, B., Makowska, K., Zdanowicz, K., Wittekoek, B., Pandrea, P., Sieńko, R., Schauber, P., Topolnicki, M., Zachert, H. (2024b). Distributed Fibre Optic Sensing (DFOS) in 3D small-scale tests on steel-reinforced piled embankments. In: *Proc. ECPMG 2024*, Delft, Netherlands.

Zhang, Z., Wang, M., Ye, G. B. and Han, J. (2019). A novel 2D-3D conversion method for calculating maximum strain of geosynthetic reinforcement in pile-supported embankments. *Geotextiles and Geomembranes*, 47 (3) 336–351. DOI: 10.1016/j.geotexmem.2019.01.011.